JOURNAL OF THERMOPHYSICS AND HEAT TRANSFER
Vol. 15, No. 4, October–December 2001

Experimental Evaluation of Triangular Microgrooved on a Condensing Surface

R. Barron-Jimenez*
Texas A&M University, College Station, Texas 77843-3123
and
G. P. Peterson†
Rensselaer Polytechnic Institute, Troy, New York 12180

The addition of microgrooves to a condensing surface has been proposed to reduce the film thickness to increase the condensation heat transfer coefficient. Microgrooves promote the removal of condensate via the capillary pressure induced by the difference in curvature of the meniscus formed in the groove. Triangular microgrooves of different apex angles (45 and 60 deg) and width (300 and 500 μm) were machined on several copper plates (140 × 25.4 mm), and the resulting film condensation was observed at a macroscopic scale. Experimental results demonstrated the beneficial presence of the grooves by achieving enhancement factors up to 2.22 in the Nusselt number. This enhancement was separated to allow determination of the individual contributions of the gravitational body force and the effect of the steam stream velocity. Visual observation of the phenomenon demonstrated that the microgrooves evaluated had an active length, but that the effect of this active length was easily obscured by the macroscopic phenomenon that produced a thick condensate film over a majority of the length of the plate. Conclusions from the current research indicated that the microgrooves were able to improve the heat transfer process, even at a macroscopic length scale, because they added an additional path through which the condensate could be removed. When conditions similar to microscale condensation were obtained, the effect of the grooves was isolated and found to be very satisfactory.

Nomenclature

a	=	microgroove spacing, Fig. 3, m
C_p	=	specific heat, J/kg K
D_h	=	hydraulic diameter, m
H_r	=	microgroove's depth, m
h	=	condensation heat transfer coefficient, W/m^{2}K
$\bar{h}$	=	overall condensation heat transfer coefficient, W/m^{2}K
k	=	thermal conductivity, W/mK
l	=	length, m
Nu_l	=	Nusselt number based on length
$\bar{N}u_l$	=	overall Nusselt number based on length
n	=	number of microgrooves on the plate
$\dot{q}''$	=	heat flux, W/m^2
Re_{Dh}	=	steam flow Reynolds number, based on vapor tunnel hydraulic diameter
S	=	microgroove spacing, Fig. 3, m
T	=	temperature, K
$\dot{V}$	=	volumetric flow rate, m^3/s
W	=	microgroove width, m
w	=	width, m
γ	=	volumetric division factor of the cooling stream
ΔT	=	relative temperature, K
δ	=	film thickness, m
ρ	=	density, kg/m^3
θ	=	microgroove apex angle, deg
Ω	=	tilting angle of test module with respect to the horizontal, deg

Subscripts

c	=	cooling
entrance	=	entrance region
film	=	condensate film
paper	=	paper region
plate	=	plate
region	=	either paper or entrance region
vapor	=	vapor

Presented as Paper 2000-0965 at the 38th Aerospace Sciences Meeting, Reno, NV, 10–13 January 2000; received 3 February 2000; revision received 4 June 2001; accepted for publication 5 June 2001.

*Research Assistant, Department of Mechanical Engineering.
†Provost, Department of Mechanical Engineering, Aeronautical Engineering and Mechanics. Fellow AIAA.

Introduction

OVER the course of the last decade, there has been an increasing interest in the transport phenomena occurring at very small length scales. Much of the interest in this area has been driven by the electronics industry and its constant search for smaller, faster, and more powerful integrated circuit devices. In addition, advances in microelectromechanical systems technology have resulted in a wide variety of applications for microscale devices that include both energy exchange and chemical conversion systems.

Research into the fundamental phenomena of microscale heat transfer has generated a significant amount of information in all three principal areas of heat transfer, including conduction, convection, and radiation heat transfer. Efforts have been devoted to both the analytical and experimental evaluation of heat transfer in microstructures for cooling silicon chips in which there is flow through microchannels. Duncan and Peterson[1] summarized numerous studies of forced convection in microchannels and the heat transfer occurring in different configurations of micro heat sinks and micro heat exchangers incorporated into electronic components. One particularly important aspect of microscale phenomena on which very little work has been done is that of condensation. Film condensation, one of the important heat transfer phenomena occurring in many types of heat transfer equipment, is of particular interest in compact heat exchangers and other microscale devices.

Nusselt first analyzed film condensation controlled by the gravitational body force in 1916. Many investigators[2] have expanded Nusselt's theory to take into account the effects of noncondensible

gases, interfacial shear, superheating, property variations, diffusion and nonuniform gravity forces on film condensation.

Gregorig[3] first introduced the concept of using the surface tension forces to drain condensate from the fins in a fluted tube. The surface tension on a curved surface may induce a pressure gradient that exceeds the gravity-induced body force. In some cases surface tension forces may be used to thin the condensate film at the tips of fins and to promote the removal of condensate through the flow channels, thereby enhancing the condensation heat transfer process. Several important contributions[4–6] have been made to help to understand the role of surface tension in this condensate removal process.

External condensation enhancement was achieved by means of integral finned tubes, and the fin geometry has been investigated extensively to optimize the fin performance. Additional efforts to remove liquid from the flooded regions have promoted the application of external disks,[7] longitudinal drainage strips,[8–10] rotating devices, and other methods.

The present research proposes the effective utilization of the pumping capability of surface tension to reduce the condensate film and, by so doing, to increase the condensation heat transfer coefficient. The configuration evaluated here is a series of triangular microgrooves machined on the surface of a flat copper plate.

In 1995, Peterson and Ma[11] investigated the capillary flow in microgrooves and found that there exists an optimum geometry that can provide the maximum heat transport capability for a micro heat pipe of a given shape. This work indicated that the thermal resistance occurring at the condensing surface plays an important role in establishing the operational limits of these devices.

It is well known that the thermal resistance occurring during film condensation depends primarily on the thickness of the liquid condensate film. Decreasing this thickness will enhance the condensation heat transfer coefficient and substantially improve the efficiency of the overall heat transfer process. In many instances, it may be possible to use surface tension to reduce the film thickness. Previous investigations have shown that, when the tip of a groove comes into contact with a wetting liquid, the surface tension forces cause the liquid to flow to the bottom of the grooves, resulting in a thinning of the condensate film at the tip of the groove. As the length scale gets smaller, the role of the interfacial forces becomes more important, particularly when the condensate film thickness is less than 100 nm (Ref. 12). At these length scales, the film condensation and condensate flow in the microchannels will be governed not only by gravity and surface tension forces, but also by the interfacial forces such as the disjoining pressure.

Regardless of whether one is trying to utilize microgrooves to reduce the amount of liquid retained in grooves to improve the overall heat transfer coefficient in the film condensation process or to retain liquid in the grooves in applications such as micro heat pipes, it is clear that a better understanding of the fundamental phenomena that govern the condensation process in microgrooves could lead to enhanced performance in a wide variety of applications.

The current investigation is focused on experimentally typifying the performance of microgrooves in film condensation on horizontal and near-horizontal copper plates. The objective is to determine the effect of the microgroove geometry and dimensions in an effort to optimize the condensation heat transfer coefficient, as well as to evaluate the bulk effect of the presence of microgrooves on the plate.

Experimental System and Methodology

To evaluate the combined and individual roles of the gravitational, capillary, and interfacial forces, an experimental study of condensation on four microgrooved plates was conducted. As discussed earlier, microgrooves have the ability to promote the removal of condensate from the surface via the capillary pressure induced by the difference in curvature of the meniscus formed in the groove. Reducing the condensate film thickness results in an improvement in the condensation heat transfer coefficient.

Experimental Apparatus

The experimental system was designed to determine the condensation heat transfer in a series of microgrooved plates oriented horizontally and near horizontally. The experimental apparatus, shown schematically in Fig. 1, consists of three major sections: 1) a test module, 2) a steam loop, and 3) a cooling loop.

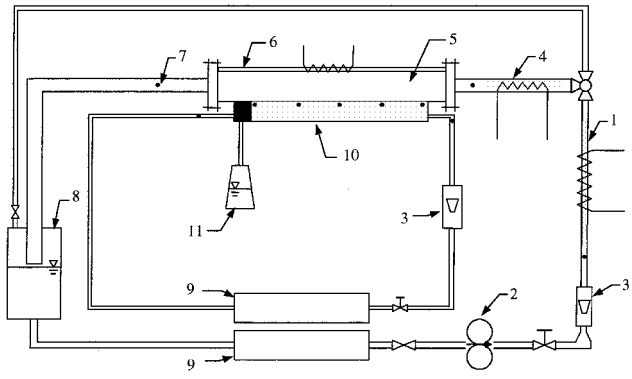

Fig. 1 Experimental apparatus schematic: 1) boiler, 2) pump, 3) rotameter, 4) super-heater, 5) vapor tunnel, 6) observation window, 7) thermocouples, 8) direct-contact condenser, 9) constant-temperature bath, 10) microgrooved plate, and 11) condensate removal unit.

The steam that flows through the test module is generated in the steam loop (external loop, Fig. 1). This steam loop consisted of a closed-loop boiler test module condenser through which steam is initially produced. This steam in the loop, which is produced through the vaporization of ultrapure water, flows from the boiler to a condenser, where is then returned to the boiler. Ultrapure water was chosen as the working fluid because of its high latent heat and high surface tension. Future research will involve the use of methanol to detect the role of surface tension during the process. A gear suction pump in the loop was used to assure a steady supply of water to the boiler and minimized flow pulsations within an accuracy of 2%.

Internal convective boiling in a horizontal tube was used to generate the steam. The 92-cm-long tube was made from Inconel® 600 a Ni/Cr/Fe alloy, and the entire tube served as the electrical heater due to its very low electric resistivity. In addition, the reaction of Inconel with water at high temperatures is essentially nonexistent, thereby eliminating the production of noncondensible gases. Each end of the Inconel tube was connected to the electrodes of an arc welding machine that operated as a current-regulated power supply. This boiling system was effectively used to generate saturated vapor at a constant mass flow rate. The actual volumetric flow rate was measured using a rotameter while the flow was still in liquid phase.

During the process, the saturated vapor flows through the superheater section, where additional heat is added to the vapor stream to achieve superheated conditions up to 135°C. For the tests where the vapor conditions were required to be at saturation, the superheater and the electrical heaters on the ducts were used only to compensate for heat losses, avoiding condensation as the vapor flowed through them. The axis of the superheater tube was aligned with the longitudinal axis of the vapor tunnel and had a small observation window so that the vapor coming into the test module could be observed. This window allowed the vapor to be visually monitored and was used to ensure that there was no condensation of the vapor upstream of the test section.

In the test module, a portion of the vapor was condensed and then was removed by the condensate removal unit. The remaining vapor exited the test module and was condensed on the direct contact condenser. This type of condenser allowed the system to be maintained at the atmospheric pressure (101.35 kPa) during the entire operation. The condenser was located away from the test module to diminish the influence of the pressure drop resulting from condensation. Condensed liquid from the condenser was returned to the constant temperature bath reservoir to be reintegrated into the cycle at 20°C.

The purpose of the cooling loop (inner loop in Fig. 1) was to maintain the test article at a constant preset temperature during the test period. The cooling bath was used to set the cooling water temperature for each experiment and to control it within ±0.02°C. The test module of the experimental apparatus, shown in Fig. 2,

Table 1 Dimensions of the tested triangular microgrooves

Parameter	Plate 0	3	5	6
W, mm	0	0.33	0.67	0.69
θ, deg	0	60	60	45
a, mm	25.4	2.59	2.46	2.45
S, mm	0	1.47	1.13	1.11
H_r, mm	0	0.21	0.48	0.60
n	0	12	12	12
D_h, mm	0	0.14	0.32	0.33

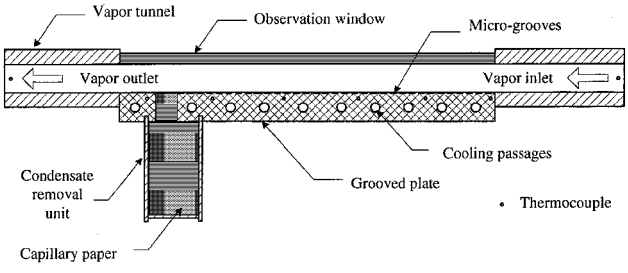

Fig. 2 Test module schematic.

consisted of a 322.58-mm^2 cross-sectional area, vapor tunnel constructed from Teflon®. The length of the tunnel entrance (127 mm) was calculated to assure fully developed steam flow, when it reached the microgrooved plate test article. Another feature of this vapor tunnel was the observation window. A piece of Pyrex® glass was attached to the test module on top of the copper plate to allow visual observation of the liquid behavior on the microgrooves and to determine the condensation regime, draining fluid pattern, and vapor flow phenomena. To prevent condensation on the observation window, a stainless-steel foil heater was attached to the external top surface and a small amount of heat was added.

Because the condensate removal rate directly affects the condensation rate and thereby the condensation heat transfer, an experimental technique, previously developed by Ma and Peterson,[13] was employed. Based on a maximum capillary capability analysis,[11] the maximum capillary pumping head depends only upon the variation of the meniscus radius of curvature. For this reason, the condensate removal unit was intended to maintain a minimum and constant meniscus radius of curvature at the exit of the grooves. The condensate removal unit was composed of capillary paper to remove the condensate completely at the exit of the grooves.

To provide plate cooling, nine circular 4.57-mm-diam passages were drilled through the copper plate transversely to the plate. The interconnection of these passages was done according to the plate cooling requirements so that the temperature profile along the plate was as flat as possible.

To reduce heat losses, the vapor path from the boiler's outlet to the test module's exit was covered with a 25.4-mm-thick high-temperature fiberglass insulation blanket (not shown in Figs. 1 and 2).

Grooved Plates

Each test article was prismatic, 12.7 mm in height, 25.4 mm in width, and 170 mm in length made in copper. On the top surface of the plates, 12 V-shaped microgrooves, 139.7 mm long, were machined. The initial investigation was conducted using triangular grooves with 45- and 60-deg apex angles and widths of 300 and 500 μm. To ensure the accuracy of the grooves once machined, each groove was measured using an optical profilometer. Table 1 shows the dimensional average characteristics of the grooves tested and refers to Fig. 3.

Although the hydraulic diameter of the microgrooves is the value normally used to describe the physical shape of the groove, throughout this paper the plate number will be used to refer to the specific set of grooves discussed. This convention is adopted to avoid confusion among grooves if plates with grooves having a similar hydraulic diameter are used. As observed in Table 1, plate 0 does not contain any microgrooves. This smooth plate was manufactured and included in the test matrix to provide a reference for identifying the microgroove effect.

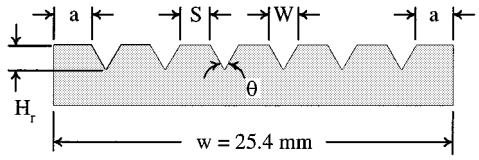

Fig. 3 Microgrooves geometry.

Thermocouples on the copper plate were used to monitor its superficial temperature and to assure that steady state was achieved. At 1.27 mm from the microgrooved surface on a 10-node grid, 10 T-type thermocouples were embedded symmetrically distributed over the entire microgrooved surface. Two more thermocouples were located in the vapor tunnel, one at the entrance and the other at the exit. These thermocouples, spatially centered in the cross section of the vapor tunnel, monitored the temperature of the incoming/outgoing steam. Three thermocouples were used to measure the relative temperature increment in the cooling water. No other sensors were used in the test section, and only the temperature was monitored during the experiments.

Experimental Procedure

When plates 0, 3, 5, and 6 and the resulting experimental data are used, comparisons of the microgroove geometry (width and apex angle) can be made. The inclusion of plate 0, the smooth plate, was helpful in identifying the real benefit of the microgrooved surface.

Each plate was tested in a test matrix of 24 different test conditions. The steam flowing over the test plate was coded with roman numerals indicating vapor velocity of I) 0.85 m/s ($Re_{Dh} = 724$), II) 3.78 m/s ($Re_{Dh} = 3186$), or III) 4.32 m/s ($Re_{Dh} = 3646$). At these conditions (as indicated by the Reynolds number based on the vapor tunnel hydraulic diameter), the flow was set in the laminar and turbulent regimes.

The tilt angle Ω was changed from 0 to 5 and 10 deg from the horizontal in the downhill direction, the direction in which the gravitational force will help the condensate fall toward the condensate removal unit. For the tilt tests, vapor flowed at rates I and III (laminar and turbulent regimes) for each of the cooling loop set temperatures. The water temperature on the cooling loop was set to 20, 40, and 60°C. In this way the plate temperature could be substantially changed. Notice, however, that the actual plate temperature is not equal to the set temperature of the cooling loop due to the heating of the plate from the condensing vapor.

For each test, careful attention was given to plate preparation and mounting into the test module because preliminary results showed this to be of critical importance. For each test, the plate was cleaned to remove dust, oils, and tarnish from the surface. The cleaning process was of primary importance because it is the mechanism that assures water wettability of the copper surface, so that film condensation can be achieved. Barron-Jimenez[14] has given an accurate description of the cleaning process, which is a modification of the procedure suggested by Lyman.[15] When the plate was clean, meaning the surface had the desired distinguishable copper color, it was mounted on the test section, connections and seals were completed, and the orientation of the plate was checked. Running compressed air through the test section helped to maintain the integrity of the surface, and film wise condensation was easily obtained for several tests until the plate had to be removed and cleaned once again.

By running both the steam and cooling loops for approximately 35 min, the experimental system stabilized and achieved steady state, that is the plate temperature, the vapor flow rate, and the condensate flow removal rate all reached constant values. Once steady state had been achieved, the tests and data acquisition were continued for 15–20 min, with data taken periodically to provide confirmation of the test results.

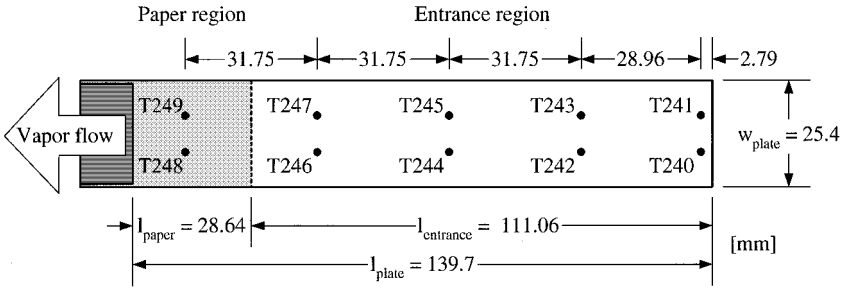

Fig. 4 Paper and entrance regions, plate bottom view.

Analysis

The measured effect of the grooves was supported by visual observation of the condensate film thickness. Film reduction was detected in the exit region of the microgrooves, close to the condensate removal unit. The heat transfer in this film-reduced region was expected to be larger than that transferred in the rest of the plate. To account for this difference in the heat transfer coefficient, the plate was divided into two regions. The paper region and the entrance region were arbitrarily defined according to the symmetry of the cooling passages and thermocouple distribution.

Figure 4 presents the schematic of the region's distribution. The entrance region represented 79.5% of the superficial area of the microgrooved plate; eight thermocouples were located in this region. Seven cooling passages in this region and two in the paper region allowed the plate temperature to be held constant during the test periods. Although different in magnitude, the surface temperature reached at steady state presented fluctuations with a standard deviation of approximately 0.85°C at any region.

Under the assumption of constant surface temperature, the condensation heat transfer coefficient for each region was obtained from Newton's law of cooling [Eq. (1)], and the heat rate transferred to each specific region could be determined by performing an energy balance on the cooling water of the corresponding region:

$$h_{\text{region}} = \frac{\dot{V}_{c,\text{region}} \rho C_p \Delta T_{c,\text{region}}}{l_{\text{region}} w_{\text{plate}} (T_{\text{vapor}} - T_{\text{region}})} \tag{1}$$

Note that the effective condensation area was considered to be the projected superficial area of the plate because condensation occurred on the top of the condensate film. The cooling water volumetric flow rate for each region was experimentally related to the measured total volumetric cooling flow by a division factor estimated to be $\gamma = 0.475 \pm 1.5\%$:

$$\dot{V}_{c,\text{paper}} = \gamma \dot{V}_c \tag{2a}$$

$$\dot{V}_{c,\text{entrance}} = (1 - \gamma) \dot{V}_c \tag{2b}$$

Dividing the microgrooved plate into two regions was helpful in that it allowed the different behaviors of the phenomenon in those regions to be quantified. However, to view the experiment as a whole, the overall condensation heat transfer coefficient was calculated as

$$\bar{h} = \frac{\dot{V}_c \rho C_p \Delta T_c}{l_{\text{plate}} w_{\text{plate}} (T_{\text{vapor}} - T_{\text{plate}})} \tag{3}$$

In general, the experimental uncertainty of the calculated heat transfer coefficients was less than 25% for either the paper or the entrance regions and 31% for the overall plate.

Dimensionless heat transfer coefficients were necessary to allow comparison of the results in each region, due to the relatively arbitrary selection of the length of these regions. Nusselt numbers for each region, as well as the overall plate, were calculated using

$$Nu_{l,\text{region}} = h_{\text{region}} l_{\text{region}} / k \tag{4a}$$

$$\bar{N}u_l = \bar{h} l_{\text{plate}} / k \tag{4b}$$

An estimation of the film thickness could be determined by assuming conduction through the film as

$$\delta = k_{\text{film}} \frac{T_{\text{vapor}} - T_{\text{plate}}}{\dot{q}''_{\text{region}}} \tag{5}$$

The film thickness was calculated at 10 locations, one at each point where the plate thermocouples were embedded. The heat flux was then determined depending on in which region the thermocouples were located. Although results from this approach were not experimentally corroborated by any measurement, visual observation of the condensate film helped to validate the calculated general shape of the condensate layer.

Results and Discussion

As already mentioned, the objective of the experimental program was to characterize and identify the effect of microgrooves on condensing surfaces and to determine the impact these grooves could have on the condensation heat transfer coefficient. Experimental measurements were made to compare the overall condensation heat transfer coefficients on plates with different groove sizes, at various flow conditions and tilt angles, which changed the effect of the gravitational body force. Before the data reduction and analysis, an uncertainty analyis was conducted and an energy balance was performed in which the latent heat released and the sensible heat increment in the cooling water stream were compared. This process indicated that the maximum heat loss was 13% at this level, which occurred for the tilt tests (especially for plates 0 and 3) at low vapor velocity, and, hence, these tests were identified as unreliable. Visual observation of these tests provided further indication that condensation occurred in a reduced portion of the plate so that the presence of air in the tunnel could be assumed, leading to a completely different testing situation. Therefore, these results were not considered in the discussion.

Condensation Heat Transfer Coefficient

With the validated experimental results, data were processed to obtain the condensation heat transfer coefficient. Recall that the superficial area of the copper plate was divided into two regions, paper and entrance. For each region the condensation heat transfer coefficient as well as the overall coefficient for the entire plate were calculated.

Consider the horizontal tests ($\Omega = 0$). Figure 5 presents the results for the Nusselt number for each region at the different Reynolds numbers Re_{Dh} tested. It can be observed that for lower Re_{Dh}, the dimensionless heat transfer coefficient had similar orders of magnitude for any plate at any region. Even for $Re_{Dh} = 3646$, the data fell within the experimental uncertainty. Thus, the effect of the microgrooves was not detected at any region.

When the Reynolds number of the incoming vapor flow was increased, an increased difference between the paper and the entrance region dimensionless heat transfer coefficients was obtained. The sweeping effect of the flow over the entrance region is reflected in the Nusselt number $Nu_{l,\text{entrance}}$ increment and in the decrement of the condensate film thickness. This sweeping of the film causes liquid to accumulate in or near the paper region, decreasing the transfer of heat.

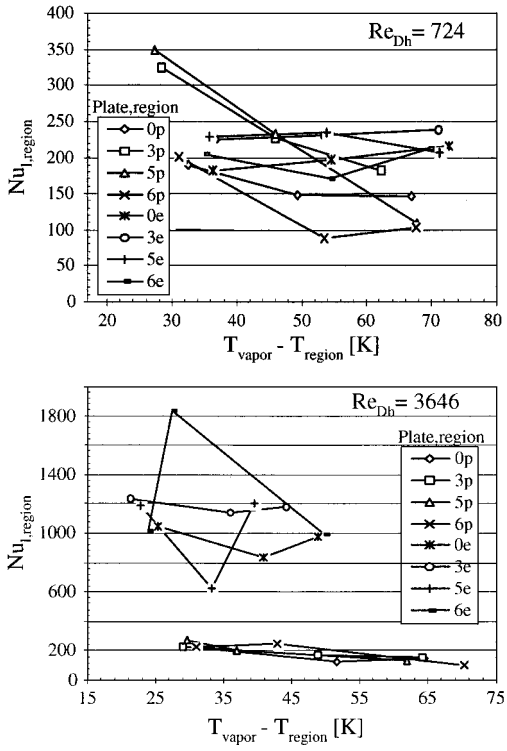

Fig. 5 Plate comparison of the Nusselt number for regions in the horizontal testing.

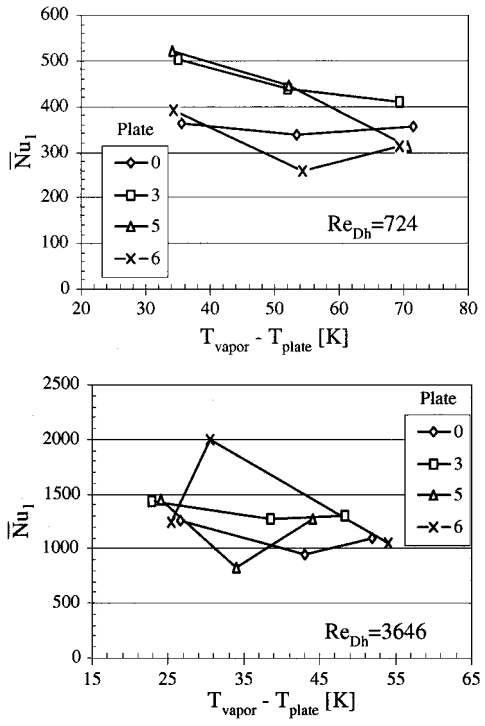

Fig. 6 Plate comparison of the overall Nusselt number in the horizontal testing.

A closer look into the special case where $Re_{Dh} = 724$ and a very low $T_{vapor} - T_{plate}$ exists in the paper region on plates 3 and 5 reveals a situation where the presence of the microgrooves dominated the phenomenon. Under these conditions, plates 3 and 5 illustrate enhancement factors in the dimensionless heat transfer coefficient obtained for plate 0 of up to 1.75. The paper and entrance regions were combined to compute the overall heat transfer coefficient. The substantially larger entrance region dominated the mixture; thus, the resulting dimensionless overall heat transfer coefficients trends were similar to the forms and trends observed in Fig. 5 for the entrance region.

Figure 6 shows the corresponding overall Nusselt number based on the entire length of the plate. These graphs are similar to the shapes for the entrance region. However, the overall dimensionless heat transfer coefficient is displaced by an average of 200, due to the effect of the capillary paper and not because of the microgrooves. This last statement is corroborated by observing the same behavior on plate 0, where no grooves had been machined. Also worth noting is the scattering of data in Figs. 5 and 6, which reflects the complicated phenomenon occurring when the effect of the grooves is not dominant.

Up to this point, the horizontal plate testing has been presented and the effect of the microgrooves has been weakly observed while checking the paper region behavior. During horizontal testing, the gravitational body force was effectively eliminated from the experiment. To include the gravity effect in the condensation phenomenon, the plate and vapor tunnel were tilted; thus, the gravitational component was proportional to the cosine of the tilting angle Ω. The tilting direction was such that the gravitational body force component would help to drain the condensate film toward the condensate removal unit.

Figure 7 presents the Nusselt number calculated in the paper and entrance regions of the plate for the tilt tests. When the data in Fig. 7 are compared, it is evident that heat transfer occurs primarily in the entrance region. For the paper region, all of the plates behaved in a similar manner. The similar behavior of the paper region and the reduction in the dimensionless heat transfer coefficients are the result of the added effect of gravity that tended to move liquid toward the paper region, allowing it to accumulate there. This mechanism

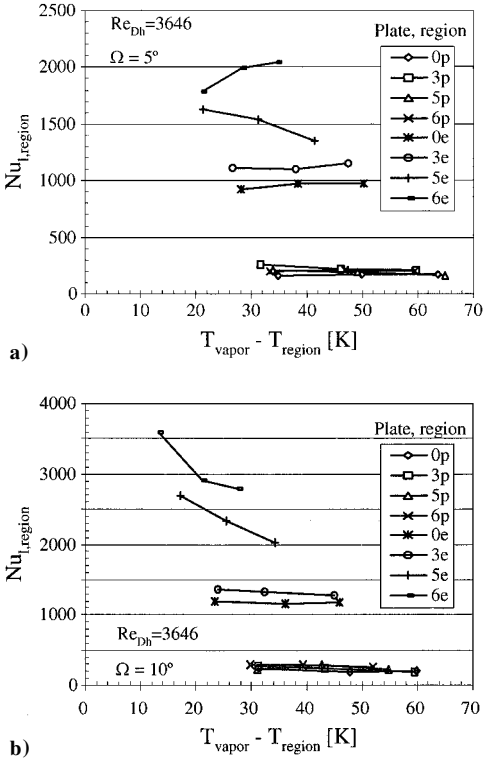

Fig. 7 Plate comparison of the Nusselt number for regions in the tilted testing.

had a similar film thinning effect in the entrance region, as did the increment of the Reynolds number of the vapor flow.

The effect of the microgrooves was readily observed in the entrance region producing the vertical displacement of the top lines of Figs. 7a and 7b. Even considering the experimental uncertainty, it is apparent that, as the tilt angle increases, the gap between the Nusselt number for plates 5 and 6 and the Nusselt number obtained for Plates 0 and 3 increases. Then, for turbulent vapor flow, the increment of

the dimensionless heat transfer coefficient can be readily observed. Here, the calculated values differed enough so that the experimental uncertainties do not overlap, allowing the positive effect of the microgrooves to be easily observed.

The overall dimensionless heat transfer coefficient was calculated and is presented in Fig. 8. Figures 8a and 8c show the overall Nusselt number for the lower values of Re_{Dh}. Recall that results from these tests were classified as unreliable based on the energy balance. It is apparent, however, that the behavior among plates was similar, reflecting that the test conditions were different from the other experiments and that the microgrooves did not constitute an important factor.

Comparisons of the tests at $Re_{Dh} = 3646$ (Figs. 8b and 8d) were made because the enhancement factor of the microgrooves had been isolated. Table 2 presents the average of the enhancement factors for the microgrooved plates with respect to the smooth plate that were observed for the values given in Fig. 8.

Plate 3 had a relatively small groove when compared with grooves 5 and 6. In groove 3, the cross-sectional area was 21 and 16.7% smaller, respectively. Thus, it is clear that plates 5 and 6 had an increased capability to remove condensate from the plate. For the tilt tests at high Re_{Dh}, it was clear that the bigger the microgroove was, the better the overall improvement in the condensation process. For these test conditions, plate 6 demonstrated the ability to increase the overall Nusselt number by a factor of 2.22 times the performance of the smooth plate. Plate 5 showed a scalable factor of 1.77, whereas plate 3 improved by a factor of 1.21.

To determine the enhancement factor due to the gravitational body force, the data presented in Fig. 8 were compared individually for each plate. Comparison among the overall heat transfer coefficients for corresponding conditions led to the enhancement factors summarized in Table 3.

Table 2 Microgroove enhancement factor on the overall Nusselt number, with respect to plate 0

	Plate		
Ω, deg	3	5	6
5	1.21	1.45	1.81
10	1.12	1.77	2.22

Visual Observations

Visual observation of the phenomenon provides insight into what actually happened during tests, and became an important tool that helped to determine the correct wetting characteristics of the plate, the satisfactory inlet steam quality, the condensate film stability, and other experimental performance characteristics that allowed successful completion of the experimental work. However, visual observation is not a qualitative tool, is highly dependent on the environmental conditions, and is not qualitatively precise. However, recording of visual observations allowed the condensation pattern tendencies and performance of the microgrooves to be established. For instance, in the unreliable experiments, observation of the phenomenon showed a large dry area where condensation did not occur.

All of the preceding results were supported by the film pattern observed. The smooth plate always showed a relatively thick and continuous condensate film over the entire plate.

Modifications to the condensate film were observed when the microgrooved plates were tested. For experiments at high steam velocity, the vapor flow swept the condensate film at the entrance region accumulating it in the paper region; the response of the Nusselt number in those regions is shown in Fig. 5. This condensation pattern was improved and made more evident by the tilt of the plate; however, as the microgroove cross-sectional area increased, the groove was able to remove more liquid from the flat solid surface, thus reducing

Table 3 Gravity component enhancement factor on the overall Nusselt number, with respect to horizontal testing

		Ω, deg	
Plate	Re_{Dh}	5	10
0	3649	1.02	1.25
3	3828	1.00	1.14
5	3459	1.42	2.15
6	3647	1.51	2.28

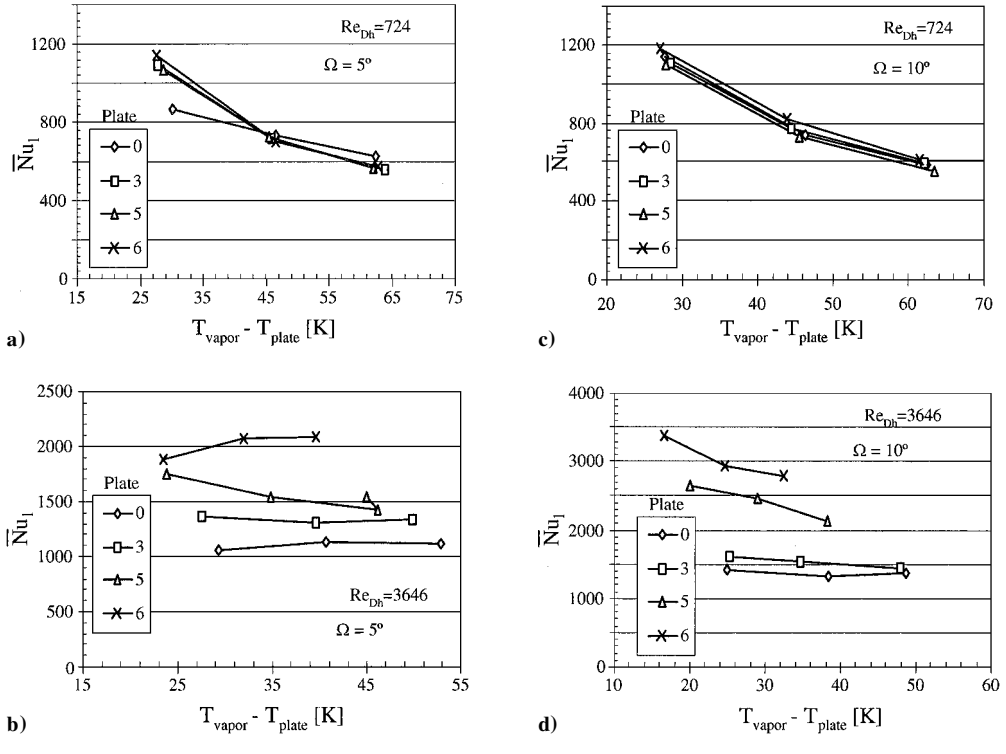

Fig. 8 Plate comparison of the overall Nusselt number in tilted testing.

the thickness of the film even more. This mechanism allowed the microgroove to enhance both the heat transfer coefficient and the condensate drainage.

Examination of the data obtained from plate 6 clearly shows the improvement caused by the specific pattern characteristics. In the film observed in the tilt tests on plate 6, the meniscus formed on the microgroove mouth was detected. Reduction of the condensate film (due to tilting and high steam velocity) to this level accounted for the larger enhancement factors of the heat transfer coefficient obtained. In this pattern, microscale condensation was achieved at the entrance region of the microgrooves (whose length was comparable to the entire plate length).

Through visual observation, a similar condensate film was not easily observed in plate 5 but indeed occurred. By calculating the film thickness δ, all of these observations can be quantified. The film thickness was computed by assuming conduction through the film [Eq. (5)]; the calculation can be reliable only at the thermocouple location in the plate. The results obtained carried the same uncertainty level as the condensation heat transfer coefficients.

In the axial direction, the plate presented a temperature profile, so that the axial variation of the heat transfer coefficient resulted in a standard shape for the condensate film. Figure 9 shows three typical shapes of the calculated film over the microgrooved plates.

Shape S1 was characteristic of the low Reynolds number flow for condensation over the horizontal plate. This shape indicated the absorbing effects of the paper and the drainage effect of the grooves, which reduced the condensate film in the paper region. Shape S2 was also present on the horizontal tests at moderate values of Re_{Dh}; for this case, the film was swept away by the incoming flow. Shape S3 was a magnification of shape S2 because it was present in horizontal tests for the highest values of Re_{Dh} tested and was always obtained in the tilt tests. On shape S3, the leading edge of the film was swept away, and liquid accumulated at the trailing edge. The calculated condensate film was not thicker than 0.2 mm for the flat portion or 1.6 mm for the thicker film of shape S3. At these orders of magnitude, it is hard for visual observation to detect fine differences, as was the case for the film patterns of plate 5.

Shape S1 shows an abrupt film thickness reduction in the paper region. This behavior was detected through visual observation during horizontal tests at low Re_{Dh} on plates 3, 5, and 6. The film reduction was observed because the condensate film reduced so much that the groove meniscus was exposed to the steam. The approximate distance along the groove through which this pattern was seen was called the microgroove active length. The active length occurred on the paper region and so it was measured from the groove exit. In general, plate 3 had 6–13 mm active length. When comparing the patterns on plates 3 and 5, it was readily observed that the active length of larger microgrooves was as much as three times larger.

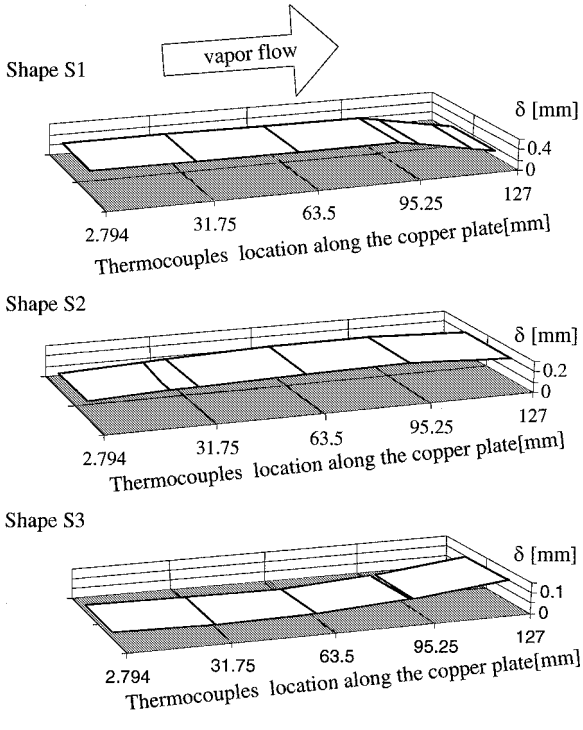

Fig. 9 Three typically computed condensate films.

It was in this active length where the microgroove pumping capability was able to dominate the phenomenon leading to microscale condensation conditions. Unfortunately, the active length was smaller than the paper region and so its effect was not reflected in the heat transfer coefficient. Moreover, due to the small number of thermocouples in the paper region, the calculation of the film thickness did not reflect the exact conditions observed. Note that similar conditions for microscale condensation were achieved on a significantly larger portion of the plate for the tilted tests, leading to the reported improvement in the overall heat transfer coefficient.

Condensate Removal

Machining microgrooves on the surface of the plates was done to provide a means of draining the condensate. Condensate collection was done as an indicator of the effect of the grooves presence. For each test, the condensate removal unit collected the condensate deposited on the copper surface during the testing period (while steady state was maintained).

It was assumed that during steady state the condensate removal rate remained constant and equal to the condensation rate. The test section was not flooded during the time required to reach steady state or during the actual tests, implying that no liquid water was accumulated and all of the condensate was removed. This assumes that the absorption capability of the capillary paper was enough to remove as much water from the liquid film as it condensed. The experimental uncertainty of the condensate removal was calculated to be 0.24%, and the energy balance demonstrated that the earlier assumption was fulfilled during testing.

However, the condensate removal rate did not constitute an indicator of the microgroove's presence as it was meant to be. The principal reason for this failure was the design of the condensate collection. With the described methodology, all of the condensate was collected, and there was no difference in the means by which the condensate was collected.

The mechanisms by which the condensate reached the capillary paper were 1) the microgrooves, 2) the wall channel described by Barron-Jimenez et al.,[16] 3) the capillary paper absorbing directly from the film that contacts it, as in the case of the smooth plate, and 4) condensation over the capillary paper, which had a surface in contact with the steam that represented 9% of the copper plate surface.

Experimental differentiation of the amounts of condensate from these different sources is quite complicated; however, minor changes in the experimental design could greatly assist in this process.

Conclusions

The principal objective of this investigation was to evaluate experimentally the performance of the microgrooves during film condensation over a copper surface. The purpose of the microgrooves was to provide an effective means for removing condensate from the surface, thus reducing the condensate film and enhancing the heat transfer process. Experimental results indicated that the addition of the microgrooves on the surface of the copper plate improved the heat transfer coefficient. Although some difficulties were experienced in determining the precise contribution of the microgrooves, an improvement was detected as a result of the presence of the microgrooves, with enhancement factors of 2.22 occurring when compared to a flat ungrooved plate. This enhancement results because as the vapor is condensed the meniscus radius grows at one end of the groove resulting in an increase in the capillary pressure, then the condensate is driven to the other end of the groove, where it is removed. Increasing the meniscus radius increased the thermal resistance of the film, thus reducing the heat transfer rate. To determine the precise effect of the meniscus radius, condensation had to occur

inside the microgroove, but physically the experimental apparatus was unable to detect this condensation in the grooves. Instead, a relatively thick film was obtained, and condensation occurred on top of the film, far from the microgroove scale domain. For this reason, during the tests, the microgrooves served only as an extra path through which the water could flow toward the condensate removal unit, and so the more mass it could carry the better the performance, as observed for plate 6.

The visually recorded phenomenon of the microgrooves indicated that the grooves actively reduced the condensate film thickness and that this action was enhanced by the inclusion of the gravity body force because it allowed a larger portion of the plate to be drained. For horizontal tests, the effect of the microgroove was identified by visual observations, but quantitative data indicated that its effect was obscured by the total length of the plate, which did not experience the active effect of the microgrooves.

Insight into the condensation phenomenon by evaluation of the interfacial forces, gravitational body force, and steam superheating in a surface-tension-dominated phenomenon can be obtained if condensation in the microgroove is achieved. Because of the inability of the experimental apparatus to sustain microscale condensation, it was difficult to separate out the individual contributions. However, the potential benefit of microgrooves in a condensing surface was clearly demonstrated.

Improvements to the design of the experimental apparatus will lead to one that will allow condensation in the microgrooves to be detected and measured. Improvements should be directed toward reducing the scale of the apparatus, increasing instrumentation in the paper region, and redesigning the condensate removal unit so that it will be able to identify clearly the condensate removed by the microgrooves.

Acknowledgments

The authors would like to acknowledge the support of the National Science Foundation to this project, as well as to H. Y. Hu for her important contributions.

References

[1]Duncan, A. B., and Peterson, G. P., "Review of Microscale Heat Transfer," *Applied Mechanics Review*, Vol. 47, No. 9, 1994, pp. 397–428.

[2]Zhou, S. Q., Shah, R. K., and Tagavi, K. A., "Advances in Film Condensation Including Surface Tension Effect in Extended Surface Passages," *National Heat Transfer Conference*, HTD Vol. 342, Vol. 4, American Society of Mechanical Engineers, Fairfield, NJ, 1997, pp. 173–185.

[3]Gregorig R., "Film Condensation on Finely Rippled Surface with Consideration of Surface Tension," *Zeitschrift für Angewandte Mathematik und Physik*, Vol. 5, Jan. 1954, pp. 36–49.

[4]Masuda, H., and Rose, J. W., "Static Configuration of Liquid Films on Horizontal Tubes with Low Radial Fins: Implication for Condensation Heat Transfer," *Proceedings of the Royal Society of London, Series A: Mathematical and Physical Sciences*, Vol. A410, No. 1838, 1987, pp. 125–139.

[5]Marto, P. J., "An Evaluation of Film Condensation on Horizontal Integral-Fin Tubes," *Journal of Heat Transfer*, Vol. 110, No. 4b, 1988, pp. 1287–1305.

[6]Yang, S. A., and Chen, C. K., "Role of Surface Tension and Ellipticity in Laminar Film Condensation on a Horizontal Elliptical Tube," *International Journal of Heat and Mass Transfer*, Vol. 30, No. 12, 1993, pp. 3135–3141.

[7]Mori, Y., Hijikata, K., Hirasawa, S., and Nakayama, W., "Optimized Performance of Condensers with Outside Condensing Surfaces," *Transactions of the American Society of Mechanical Engineers*, Vol. 103, No. 1, 1981, pp. 96–102.

[8]Honda, H., Nozu, S., and Mitsumori, K., "Augmentation of Condensation on Horizontal Finned Tubes by Attaching a Porous Drainage Plate," *Proceedings of the ASME–JSME Thermal Engineering Joint Conference*, Vol. 3, American Society of Mechanical Engineers, Fairfield, NJ, 1983, pp. 289–296.

[9]Yau, K. K., Cooper, J. R., and Rose, J. W., "Effects of Drainage Strips and Fin Spacing on Heat Transfer and Condensate Retention for Horizontal Finned and Plain Condenser Tubes," *Fundamentals of Phase Change: Boiling and Condensation*, HTD Vol. 38, American Society of Mechanical Engineers, Fairfield, NJ, 1984, pp. 151–156.

[10]Marto, P. J., Wanniarachchi, A. S., Cakan, O., and Rose, J. W., "Enhancement of Steam Condensation on a Horizontal Finned Tube by Using Drainage Strips," *Proceedings of the 2nd U.K. National Heat Transfer Conference*, Inst. of Mechanical Engineers, London, 1988, pp. 603–615.

[11]Peterson, G. P., and Ma, H. B., "Theoretical Analysis of the Maximum Heat Transport in Triangular Grooves: Study of Idealized Micro Heat Pipes," *Proceedings of the 1995 ASME International Mechanical Engineering Congress and Exposition*, Part 1 (of 2), American Society of Mechanical Engineers, Fairfield, NJ, 1995, pp. 185–192.

[12]Wayner, P. C., "Effect of Interfacial Forces on Evaporative Heat Transfer in a Meniscus," Final Rept. for April 1988–July 1991, U.S. Air Force Research Lab. WL-TR-91-2061, Wright–Patterson AFB, OH, 1991.

[13]Ma, H. B., and Peterson, G. P., "Experimental Investigation of the Maximum Heat Transport in Triangular Grooves," *Journal of Heat Transfer*, Vol. 118, No. 3, 1996, pp. 740–746.

[14]Barron-Jimenez, R., "Experimental Investigation of the Condensation Phenomenon in Micro Grooved Plates," M.S. Thesis, Dept. of Mechanical Engineering, Texas A&M Univ., College Station, TX, May 2001.

[15]Lyman, T., *Heat Treating, Cleaning and Finishing, Metals Handbook*, 8th ed., Vol. 2, American Society for Metals, Metals Park, OH, 1967, pp. 635, 636.

[16]Barron-Jimenez, R., Hu, H. Y., and Peterson, G. P., "Experimental Study of Condensation on Micro Grooved Plates," AIAA Paper 2000-0965, Jan. 2000.